viruses

MDPI

Article

Enhanced Antitumor Activity and Induction of Immunogenic Cell Death in NUT Carcinoma Cells by Combining Oncolytic Viruses with the Dual Inhibitor NEO2734

Fiona D. Nitschke [1], Julia Beil [1,2], Irina Smirnow [1], Andrea Schenk [1], Mary E. Carter [1,2], Ulrich M. Lauer [1,2,*] and Linus D. Kloker [1,2,*]

[1] Department of Medical Oncology and Pneumology, Virotherapy Center Tübingen (VCT), Medical University Hospital, 72076 Tübingen, Germany
[2] National Center for Tumor Diseases (NCT), NCT Tübingen, a Partnership Between DKFZ and Department of Medical Oncology and Pneumology, Medical University Hospital Tübingen, 72076 Tübingen, Germany
* Correspondence: ulrich.lauer@med.uni-tuebingen.de (U.M.L.); linus.kloker@med.uni-tuebingen.de (L.D.K.)

Abstract

NUT carcinoma (NC) is a rare exceptionally aggressive malignancy, defined by *NUTM1* gene translocations, most commonly generating a *BRD4*::*NUTM1* fusion that results in a poor prognosis and limited therapeutic options. Oncolytic virotherapy has emerged as a promising strategy for NC, and the dual bromodomain and extra-terminal domain (BET) and p300/CBP inhibitor NEO2734 has demonstrated potent antiproliferative activity. To investigate multimodal therapeutic approaches that combine epigenetic modulation with immunogenic and cytotoxic effects of oncolytic viruses (OVs), we evaluated two recombinant OVs, including the herpes simplex virus talimogene laherparepvec (T-VEC) and a measles vaccine virus (MeV-GFP), in combination with NEO2734 in four distinct NC cell lines. Viability assays revealed enhanced tumor cell reduction with all combinations, including synergistic effects with T-VEC combinations. Cell cycle analysis showed G1 arrest with NEO2734 alone, whereas its combination with T-VEC resulted in S-phase broadening and reduced G2-phase populations, consistent with replicative stress and increased cytotoxicity. Evaluation of immunogenic cell death (ICD) markers displayed elevated ATP and HMGB1 levels and increased surface calreticulin with T-VEC and NEO2734 combinations. Overall, these findings indicate that combining OVs with BET/p300 inhibitors elicits potent antitumor responses, supports synergistic interactions and immunogenicity, and warrants further investigation in multimodal therapeutic strategies for NC.

Keywords: NUT carcinoma; oncolytic viruses; virotherapy; talimogene laherparepvec; T-VEC; MeV-GFP; BET/p300 inhibitor; NEO2734; immunogenic cell death

Check for updates

Academic Editors: Arianna Calistri and Sandra Tuyaerts

Received: 15 January 2026
Revised: 7 February 2026
Accepted: 12 February 2026
Published: 20 February 2026

Copyright: © 2026 by the authors. Licensee MDPI, Basel, Switzerland. This article is an open access article distributed under the terms and conditions of the Creative Commons Attribution (CC BY) license.

1. Introduction

NUT (nuclear-protein-in-testis) carcinoma (NC) is an extremely rare, highly aggressive, and underdiagnosed squamous tumor that can affect any part of the body, particularly the head and neck region, the mediastinum and the lungs [1–4]. The disease primarily affects young adults with a median age of onset around 23.6 years [4,5].

NC arises from a single somatic gene translocation that fuses the *NUTM1* (NUT midline carcinoma family member 1) gene with various partner genes, in approximately 75% of cases with *BRD4* [3], followed by *BRD3* [6] (bromodomain containing protein 4 or 3) or *NSD3* (nuclear receptor binding SET domain protein 3) [7]. This fusion generates aberrant

NUT fusion oncoproteins, which are associated with the recruitment and activation of p300, a histone acetyltransferase. The p300-mediated hyperacetylation of histones promotes their interaction with BET (bromodomain and extraterminal domain) proteins such as BRD4 [8,9]. Consequently, extensive hyperacetylated chromatin megadomains are formed, driving strong upregulation of transcription factors like MYC, SOX12, and TP63, thereby promoting cell proliferation while blocking terminal differentiation [10–13].

Surgical resection, radiotherapy, and polychemotherapy represent current therapeutic approaches [14–17]. However, their impact on the overall survival (OS) is limited, as the median OS in NC patients remains only six to seven months [4,18].

New treatment strategies include immune checkpoint inhibitors (ICIs) used in a few reported cases, often employed in combination with chemotherapy or radiotherapy [19,20]. The observed responses are mostly transient, as NCs often display low PD-L1 expression, a low tumor mutation burden (TMB), and a "cold" tumor microenvironment (TME). Nevertheless, some cases suggest therapeutic potential [19,21–25].

Furthermore, RNA interference-based approaches and CRISPR-Cas9 gene editing have shown promise in preclinical NC models, although clinical translation has not yet followed [26–28].

Current research also focuses on the therapeutic application of small-molecule inhibitors (SMIs), including BET, p300, CDK9 or CDK4/6 inhibitors as well as histone deacetylase inhibitors (HDACis), as these specifically target epigenetic and transcriptional effects of the *NUTM1* fusion [12,29–31]. Yet, BET inhibitors demonstrated only limited efficacy in clinical studies, with modest response rates and the development of drug resistance [12,31–34]. Interestingly, combinatorial SMI approaches have shown synergistic tumor regression, as well as enhanced differentiation in both in vivo and in vitro models [12,29,30,35]. Among these, the dual p300/CBP and BET inhibitor NEO2734 exhibited markedly stronger tumor regression and improved survival in preclinical studies for NC compared with monotherapies [36]. This inhibitor is currently being investigated in a clinical trial in patients with advanced solid tumors as well as with hematological malignancies (NCT05488548).

Oncolytic virotherapy is another promising therapeutic approach for the treatment of NCs. Oncolytic viruses (OVs) selectively infect tumor cells by exploiting dysregulated signaling pathways, including impaired antiviral defense mechanisms resulting from tumorigenesis, while sparing healthy cells [37–39]. OVs further initiate immunogenic cell death (ICD), which relies on the antigenicity of neoantigen epitopes and the adjuvant effect provided by specific damage-associated molecular patterns (DAMPS) such as ATP and HMGB1 (high mobility group box 1) release as well as elevated calreticulin (CALR) cell surface expression [40]. These signals promote antigen presentation, activate T cells, and support the recruitment of additional immune cells into the tumor microenvironment [37,41,42].

It has already been demonstrated that T-VEC efficiently infects NC cell lines in vitro and causes pronounced cytotoxic effects [43]. Preclinical studies also indicate that combining T-VEC with BET inhibitors or other SMIs further enhances its antitumor efficacy [43,44]. Initial clinical observations come from a single case report in which the combination of T-VEC and an ICI (pembrolizumab) in addition to standard therapy in a NC patient led to tumor stabilization and an improvement in the patient's quality of life [45]. These observations underscore the possibility that OVs could achieve therapeutic value in multimodal approaches.

This study aimed to identify promising OV and NEO2734 combination therapies for NC by evaluating synergistic effects on cell viability and cell cycle state. Further, the hypothesis that NEO2734 influences OV-mediated ICD was studied.

In this light, we investigated a multicomponent approach involving the combination of the dual inhibitor NEO2734 with two different OVs. A recombinant measles vaccine virus (MeV-GFP), derived from the Mérieux strain, was employed based on preclinical evidence of its selective tumor tropism and oncolytic activity across diverse solid tumor models [46–48]. In addition, talimogene laherparepvec (T-VEC), a genome-edited herpes simplex virus approved by the US Food and Drug Administration (FDA) in 2015 for the treatment of unresectable metastatic melanoma, was included [49]. Monotherapies and combinatorial therapies were screened for potential synergisms in a panel of four NC cell lines by viability assays. Further, the influence of those combinations on the cell cycle state was studied. After identifying NEO2734 and T-VEC as a promising OV and SMI combination, the influence of this combinatorial treatment on ICD was assessed.

2. Materials and Methods

2.1. NUT Carcinoma Cell Lines

The NUT carcinoma cell lines 143100, HCC2429, and 690100, which all carry *BRD4*::*NUTM1* fusions, were kindly provided by Prof. Jens Siveke's group at the University Hospital Essen, Germany. The SNU-3178S cell line, carrying a *BRD3*::*NUTM1* fusion, was purchased from the Korean Cell Line Bank (Seoul National University College of Medicine, Seoul, Korea). All cell lines were cultured in Dulbecco's modified eagle's medium (DMEM; Sigma-Aldrich, St. Louis, MO, USA) supplemented with 10% fetal bovine serum (FBS; Sigma-Aldrich, St. Louis, MO, USA) in 75 cm^2 flasks and incubated at 37 °C in a humidified atmosphere with 5% CO_2. Experiments were performed using cells at low to intermediate passage numbers (passages 10–30). For the respective experiments, the cells were seeded in 6-, 24-, or 96-well plates.

2.2. Oncolytic Viruses

Two different OV constructs were used in this study. MeV-GFP, based on a commercially available monovalent measles virus vaccine (Mérieux strain; Sanofi-Pasteur, Leimen, Germany), was modified by inserting a gene that encodes for green fluorescent protein (GFP) as a reporter gene, as described by Berchtold et al. (2013) [46].

The modified herpes simplex virus type 1 (HSV-1) talimogene laherparepvec (T-VEC) was purchased as Imlygic® from the pharmacy of the University Hospital Tübingen (Tübingen, Germany). In T-VEC, the *ICP34.5* and *ICP47* genes were deleted to improve tumor selectivity, and a GM-CSF encoding gene was inserted to enhance the antitumor immune response [50].

2.3. Combinatorial Treatment of Oncolytic Viruses with NEO2734

For viral infection, multiplicities of infection (MOIs) were selected based on preliminary experiments to achieve 50–80% cell viability at 72 h post infection (hpi; Table S2). Virus stocks were thawed on ice; T-VEC was additionally sonicated for 30 s at 4 °C. MOIs were prepared in the following media: MeV-GFP in OptiMEM (Gibco, Thermo Fisher Scientific, Waltham, MA, USA) and T-VEC in DMEM supplemented with penicillin/streptomycin.

Cells were seeded 24 h prior to viral infection in DMEM with 10% FBS (2 mL/well for 6-well plates, 500 µL/well for 24-well plates, and 150 µL/well for 96-well plates). For infection, the culture medium was removed from the 6- and 24-well plates and replaced with 250 µL (24-well) or 1 mL (6-well) of infection medium. In the 96-well plates, 50 µL infection medium was added. Mock controls and wells assigned to NEO2734 treatment (Selleckchem, München, Germany) received the respective dilution medium without virus. T-VEC infected cells were incubated for 1 h, whereas MeV-GFP required 3 h. The infection medium was then replaced with cell culture media in the 6- and 24-well plates, whereas

an additional 50 µL of culture medium was added to the 96-well plates. Cells designated for NEO2734 treatment, alone or in combination with OVs, received IC_{25} (inhibitory concentration 25) or IC_{50} concentrations of NEO2734 determined in previous experiments, diluted in the same medium. Cells were subsequently incubated for 72 h (24- and 96-well plates) or 48 h (6-well plates).

2.4. Microscopy

Cell morphology, virus spread, and cell death were documented using a Leica DMi8 phase contrast and fluorescence microscope (Leica Microsystems, Wetzlar, Germany). Data acquisition was performed using Leica Application Suite X 3.7.2.22383 software. Fluorescence was recorded using a GFP filter set for MeV-GFP, whereas phase contrast imaging was performed for T-VEC and the dual inhibitor NEO2734.

2.5. Sulforhodamine B Cell Viability Assay

NC cell lines were seeded in 24-well plates for sulforhodamine B (SRB) cell viability assays. At 72 hpt (hours post treatment), the cells were washed with ice cold phosphate buffered saline (PBS; Sigma-Aldrich, St. Louis, MO, USA) and fixed with 10% trichloroacetic acid (TCA; Carl Roth, Karlsruhe, Germany) at 4 °C for at least 30 min. Next, wells were rinsed with water and dried at 40 °C. Fixed cells were stained with 0.4% SRB in 1% acetic acid for 15 min, washed with 1% acetic acid, and dried at 40 °C for at least 3 h. Dye was solubilized with 10 mM Tris (pH 10.5; Carl Roth, Karlsruhe, Germany) for 10 min, and the samples were transferred to 96-well plates in duplicates. The absorbance was measured in technical duplicates using a Tecan Genios Plus Microplate Reader (Tecan, Männedorf, Switzerland) at 564 nm.

2.6. Cell Cycle Analysis by Flow Cytometry

Cell cycle distribution was assessed by propidium iodide (PI; Thermo Fisher Scientific, Waltham, MA, USA) staining and flow cytometry. Cells were seeded in 6-well plates, treated 24 h afterwards, and harvested 48 hpt. After washing with PBS, the cells were detached with Accutase (Sigma-Aldrich, St. Louis, MO, USA), collected, and fixed in 70% ethanol at 4 °C for at least 1 h. The fixed cells were then washed twice with FACS buffer (PBS, 2% FBS, 2 mM EDTA (Lonza, Basel, Switzerland)). Next, approximately $1 - 2 \times 10^6$ cells were treated with RNAse (final concentration of 100 µg/mL; Biozym Scientific, Hessisch Oldendorf, Germany) for 15 min at room temperature (RT). Then, the cells were stained with PI (50 µg/mL) for 15 min in the dark at RT. The samples were analyzed using an Attune NxT flow cytometer (Thermo Fisher Scientific, Waltham, MA, USA) with 488 nm excitation and 574 nm emission. All flow cytometry data were analyzed using FlowJo v.10 software (FlowJo, Ashland, OR, USA). The gating strategies are shown in Figure S4.

2.7. CellTiter-Glo® Luminescence Cell Viability Assay

Extracellular ATP was quantified using a modified CellTiter-Glo® luminescent cell viability assay (Promega, Madison, WI, USA, G7571) adapted from the manufacturer's protocol [51]. The cells were seeded in 24-well plates and treated as described above. At 66 hpt (six hours before the end of treatment), the medium was replaced with serum-free DMEM, as serum may contain ATPases that could interfere with ATP measurement. After another 6 h (at 72 hpt), cell-culture supernatants were collected, vortexed, and centrifuged (12,100× *g* for 5 min). A total of 100 µL supernatant was transferred to opaque-walled 96-well plates; DMEM served as the background control. CellTiter-Glo® reagent was added 1:1, plates were shaken for 2 min and incubated for 10 min, and the luminescence was recorded using a Synergy HT microplate reader and Gen5.11 software (BioTek Instruments,

Winooski, VT, USA) with a gain setting of 135. All measurements were performed in technical duplicates.

2.8. Lumit® HMGB1 (Human/Mouse) Immunoassay

HMGB1 (high-mobility-group-protein B1) levels in cell-culture supernatants were quantified using the Lumit® human/mouse immunoassay (Promega, Madison, WI, USA, W6610). The cells were seeded in opaque-walled 96-well plates with clear bottoms and treated as described above. At 72 hpt, the supernatant volume in each well was adjusted to 80 µL by removing 170 µL of the initial 250 µL. Then, the HMGB1 levels were determined following the manufacturer's instructions [52].

2.9. Quantification of Calreticulin Exposure by Flow Cytometry

Calreticulin exposure on the cell surface was assessed by flow cytometry following an adapted protocol based on Liu et al. (2020) [53]. Cells were seeded in 6-well plates and treated 24 h later. Then, 48 hpt, cells and supernatants were collected, detached with TrypLE Express (Gibco, Thermo Fisher Scientific, Waltham, MA, USA) and washed twice with ice-cold PBS (500× *g*, 5 min, 4 °C). Cells were then stained with ViaDye™ Violet (CYTEK Biosciences, Fremont, CA, USA) diluted 1:500 in PBS for 20 min at 4 °C in the dark, washed and subsequently incubated with Alexa Fluor® 488 anti-calreticulin antibody (Abcam, Cambridge, UK) diluted 1:100 in FACS buffer (PBS with 1% FBS) for 30 min at 4 °C in the dark. After an additional washing step with FACS buffer, cells were fixed with 4% paraformaldehyde (PFA; Sigma-Aldrich, St. Louis, MO, USA)/FACS buffer (1:1, 15 min, 4 °C) and washed twice before resuspension in FACS buffer (final concentration 1–10 × 10^6 cells/mL). Flow cytometry was performed on an Attune NxT cytometer and analyzed using the FlowJo v.10 software. The gating strategies are shown in Figure S5.

2.10. Statistical Analysis

Synergy Scores were calculated using SynergyFinder+ web application (Faculty of Medicine, University of Helsinki, Helsinki, Finland) [54]. Statistical analyses were conducted using GraphPad Prism Version 10 (GraphPad Software, San Diego, CA, USA). One-way Welch-ANOVAs for inhomogeneous variances were performed, followed by Dunnett's T3 post hoc test, to analyze the cell viability and extracellular ATP levels. HMGB1 levels were evaluated using an ordinary one-way ANOVA with homogeneous variances, followed by Tukey's multiple comparisons test. Data from cell cycle analyses as well as analyses of the CALR surface expression were assessed using unpaired *t*-tests with or without Welch's correction depending on variance homogeneity. Exact sample sizes (*n*) are included in the figure legends. *p*-values of <0.05 were considered statistically significant. We expressed the level of significance with the following annotations in the figures: * $p < 0.05$, ** $p < 0.01$, *** $p < 0.001$, **** $p < 0.0001$, and *ns* = not significant.

3. Results

3.1. Combined Therapy of Dual Inhibitor NEO2734 with OVs Reduces Cell Viability of NC Cells

To investigate novel multimodal therapeutic approaches for the extremely aggressive NC, NEO2734 was combined with two different OVs, which were a measles vaccine virus (MeV-GFP) and the herpes simplex virus talimogene laherparepvec (T-VEC). Combinations were analyzed in four NC cell lines: 143100, 690100, HCC2429, and SNU-3178S.

First, preliminary tests were conducted to determine the IC_{25} and IC_{50} values of NEO2734 as a monotherapy for each cell line. Cell viability was assessed at 72 hpt using an SRB viability assay. In all four cell lines, the dual inhibitor induced a dose-dependent reduc-

tion in cell viability in the low nanomolar concentration range, confirming its previously reported therapeutic potential (Figure S1 and Table S1) [36].

Building on this, the potential of combining NEO2734 with OVs was investigated to assess whether interactions between the epigenetic modulator and virotherapy could enhance the therapeutic efficacy. To this end, each NC cell line was treated with combination therapies consisting of NEO2734 and a single OV, and the results were compared with those of the respective monotherapies using SRB viability assays at 72 hpt. Combination treatments were performed using IC_{25}/IC_{50} concentrations of NEO2734 (Table S1). The MOIs of the OVs were selected to achieve approximately 50–80% cell viability under monotherapy conditions (Table S2).

Predominantly additive to synergistic effects were observed in the combinations of NEO2734 with MeV-GFP and T-VEC (Figures 1, 2 and S3; Table S3). Overall, cell line 143100 proved to be the most sensitive to the combined treatments, particularly upon co-treatment with T-VEC (Figure 1e).

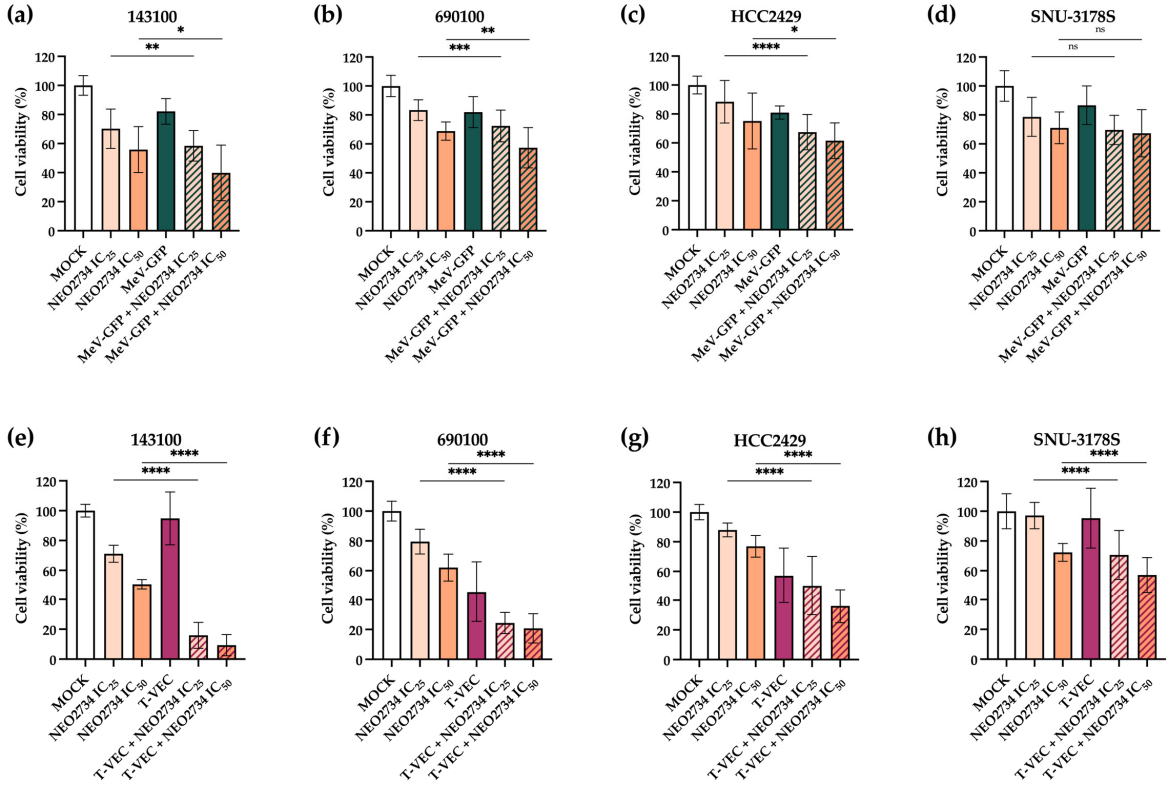


Figure 1. Combinatorial treatment of NC cells with NEO2734 and MeV-GFP or T-VEC results in enhanced reduction in cell viability: Combined treatment of different NUT carcinoma (NC) cell lines (143100, 690100, HCC2429, SNU-3178S) with the dual inhibitor NEO2734 and two recombinant oncolytic viruses (OVs), a measles vaccine virus (MeV-GFP, (**a**–**d**)) and talimogene laherparepvec (T-VEC, (**e**–**h**)), showed mostly additive effects on cell viability with MeV-GFP, as well as at least additive effects (HCC2429) up to synergistic interactions (143100, 690100, SNU-3178S) with T-VEC, compared to the respective monotherapies. Cells were incubated for 72 h and subsequently analyzed by sulforhodamine B (SRB) viability assays. All cell lines were treated with the IC_{50} or IC_{25} of NEO2734 determined in preliminary experiments (Table S1) and infected with MeV-GFP at multiplicities of infection (MOIs) of (**a**) 0.5, (**b**) 0.5, (**c**) 0.5, and (**d**) 1 and with T-VEC at MOIs of (**e**) 0.00005, (**f**) 0.0005, (**g**) 0.001, and (**h**) 0.005. Treatments were applied either in combination, individually, or cells remained untreated (MOCK). Data represent the mean ± standard deviation (SD), based on at least three independent experiments with three biological replicates ($n \geq 9$). Cell viability results are shown relative to MOCK control. * $p < 0.05$, ** $p < 0.01$, *** $p < 0.001$, **** $p < 0.0001$, *ns* = not significant.

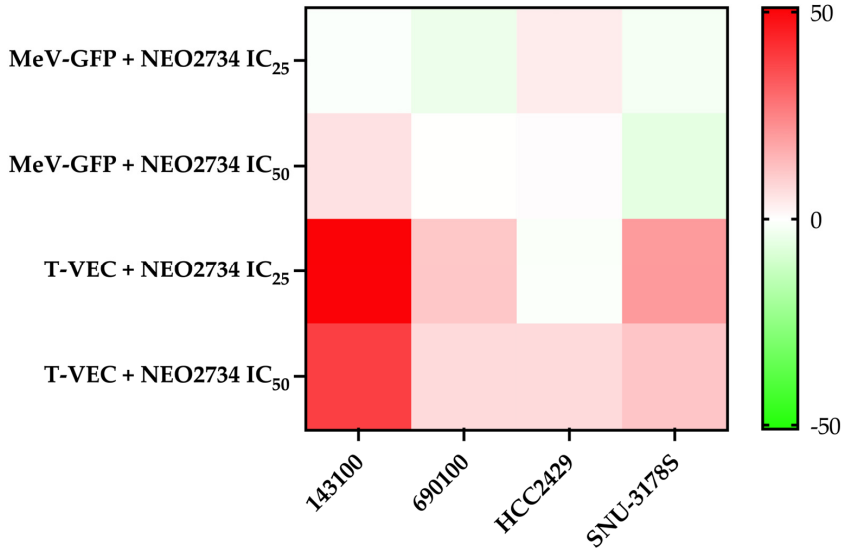


Figure 2. ZIP synergy score heatmap of OV and NEO2734 combination treatments in NC cells: The heatmap displays ZIP synergy scores for the combinations of the two OVs (MeV-GFP and T-VEC) with the dual inhibitor NEO2734, previously analyzed in Figure 1. Positive scores indicate synergistic interactions, whereas negative scores represent antagonism and values around zero reflect additive effects. Experimental conditions correspond to those of the viability assays described in Figure 1.

3.1.1. Effects of MeV-GFP Combined with NEO2734 in NC Cells

In the combination of the measles virus vaccine (MeV-GFP) with the small-molecule inhibitor NEO2734, a significant reduction in cell viability compared to respective monotherapies was observed in NC cell lines 143100, 690100, and HCC2429 ($p < 0.05$ to $p < 0.0001$; Figure 1).

Successful viral infection was confirmed in all cell lines by fluorescence microscopy based on the expression of the virally encoded green fluorescent protein (GFP) at 72 hpt (Figure S2).

These findings were reflected in the calculated synergy scores. The ZIP synergy heatmap largely showed values around zero, as cell lines 690100 and HCC2429 exhibited mean ZIP synergy scores of −2.27 and 2.14, respectively, indicating mainly additive effects. Although cell line 143100 displayed a mean ZIP synergy score of 2.48, the co-treatment with the IC_{50} concentration of NEO2734 resulted in moderate synergistic effects, with a score of 5.93. This trend was consistent across all applied synergy models (ZIP, Loewe, HSA, and Bliss), which in most cases yielded positive synergy scores, indicative of synergistic interactions (Figures 2 and S3; Table S3).

In contrast, no statistically significant reduction in cell viability was detected in SNU-3178S when compared with the respective monotherapies, although the highest MOI (1) was applied. Nevertheless, a reduction in cell viability could still be observed relative to the MOCK-treated control ($p < 0.0001$). Correspondingly, the calculated synergy scores (ZIP and Bliss) were slightly more negative (mean ZIP score −4.25), indicating weak antagonistic interactions (Figures 1d, 2 and S3; Table S3).

3.1.2. Effects of T-VEC Combined with NEO2734 in NC Cells

As T-VEC does not encode a fluorescent marker, viral infection could not be directly visualized by fluorescence microscopy. Therefore, phase-contrast images were acquired at 72 hpt to assess the changes in cell morphology. Under combination treatment conditions with T-VEC, reduced cell densities and thinned cell monolayers were observed (Figure S2).

Upon combined treatment with T-VEC, a significant reduction in cell viability compared with the respective NEO2734 monotherapies was observed in all NC cell lines

($p < 0.0001$, Figure 1). Moreover, clear synergistic effects were detected in almost all cell lines, apart from HCC2429 treated with the IC_{25} concentration of NEO2734, which rather showed an additive effect (ZIP score of −1.1; Figures 2 and S3; Table S3).

In 143100, 690100, and SNU-3178S cells, consistently positive synergy scores were observed across all applied synergy models (ZIP, Loewe, HSA, and Bliss; Table S3), indicating moderate to pronounced synergistic interactions. In these cell lines, the combination with the IC_{25} concentration of NEO2734 resulted in stronger synergistic effects than with the IC_{50} combination. Notably, 143100 exhibited by far the strongest response, with an already reduced cell viability to 15.9% following combination with the IC_{25} and to 9.3% with the IC_{50} of NEO2734 in combination with T-VEC. This was reflected by a ZIP score of 50.88 for the IC_{25} combination, whereas 690100 and SNU-3178S also demonstrated pronounced synergistic interactions in this combination, with ZIP scores of 11.15 and 20.26, respectively (Figures 1, 2 and S3; Table S3).

Based on these observations, the combination of NEO2734 and T-VEC was identified as the more promising OV and SMI combination and was, therefore, selected for subsequent investigations addressing effects on the cell cycle and markers of ICD.

3.2. Cell Cycle Analysis

To understand the mechanisms underlying the antiproliferative effects of T-VEC and NEO2734 in monotherapy and combination treatment, cell cycle distribution was analyzed 48 hpt using propidium iodide (PI) staining and flow cytometry (Figure 3). Gating for living cells was applied as shown in Figure S4, so that the cell cycle distribution resulted from the remnant viable cell population at 48 hpt.

Treatment with NEO2734 alone induced a G1 arrest in the cell lines 143100, 690100, and SNU-3178S, as indicated by an increase in the G1 fraction. In cell line 690100, this increase reached approximately 15.6% ($p < 0.05$). Although no statistically significant differences were observed in 143100 and SNU-3178S, both cell lines showed a similar trend with an approximate 10–15% increase in the G1 population.

Infection with T-VEC alone resulted in an accumulation of cells in the S phase in all three cell lines, suggesting virus-induced replication stress. However, this effect was not statistically significant.

Combination treatment led to concurrent increases in the G1 fraction relative to T-VEC monotherapy and persistent accumulation in the S phase in the cell lines 143100, 690100, and SNU-3178S. In addition, a reduction in the G2/M phase was observed following combination treatment compared with the respective monotherapies. Relative to the MOCK control, the G2/M fraction decreased by 10.8% in 143100 ($p < 0.05$), by 4.7% in 690100 ($p = 0.19$), and by 8.8% in SNU-3178 ($p < 0.05$). In the cell line HCC2429, little to no change in cell cycle distribution was observed following either monotherapy compared with MOCK control. In contrast, the combination treatment showed a slight reduction in the G2 fraction, with a decrease of 11.1%, although this did not reach statistical significance ($p = 0.21$).

Furthermore, across all NC cell lines, the combination resulted in an increase in the sub-G1 population compared with the MOCK control and most respective monotherapies. For example, in cell line 143100, the sub-G1 fraction increased to approximately 268% relative to MOCK (100%, $p < 0.05$). While the magnitude of this increase varied among cell lines, the combination treatment consistently yielded the highest proportion of sub-G1 cells, indicating enhanced DNA-fragmentation. The absolute sub-G1 percentages for MOCK controls were, on average, 2.3% in 143100, 1.6% in 690100, 1.3% in HCC2429, and 9.9% in SNU-3178S.

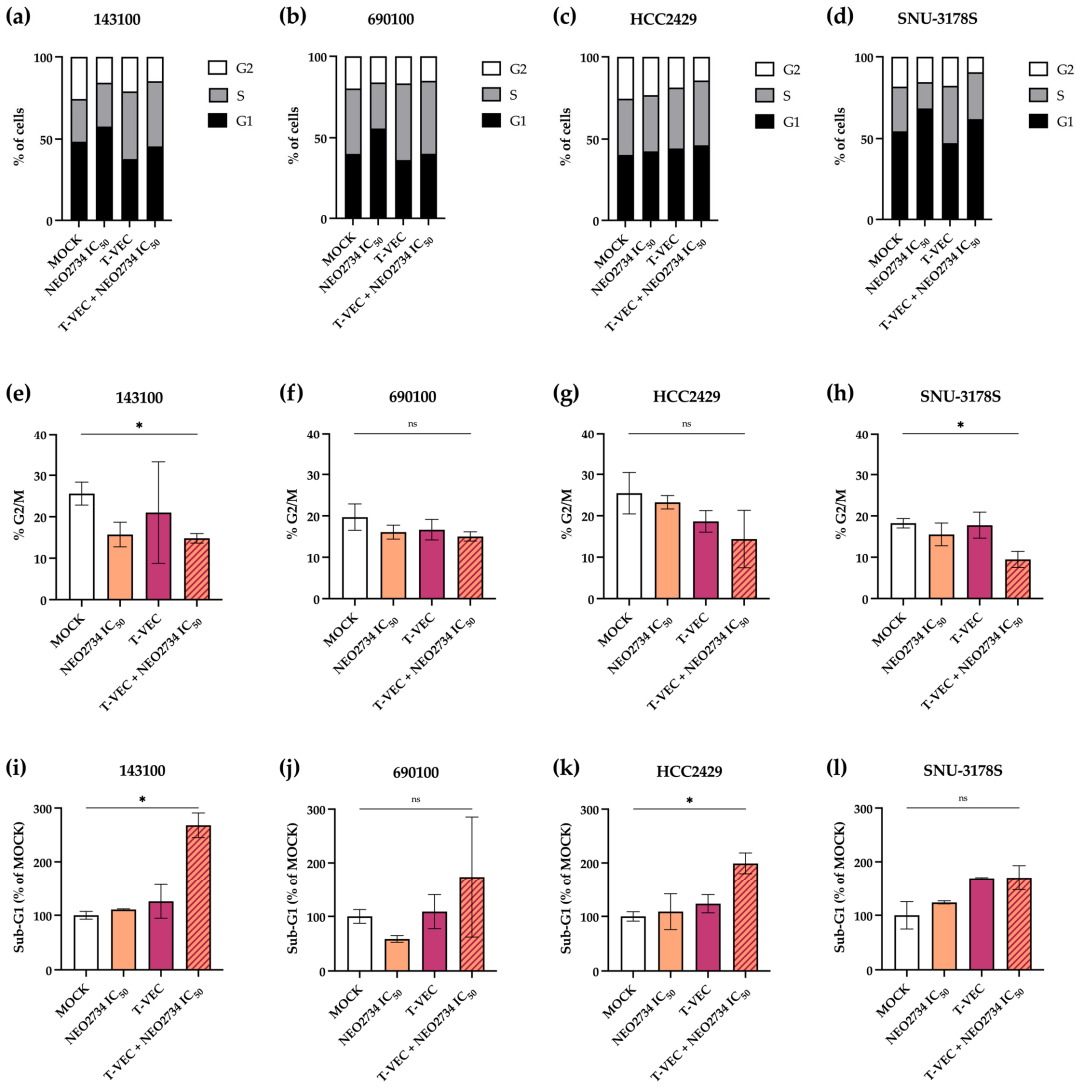


Figure 3. Reduced G2/M- and elevated sub-G1 fractions by combination treatment of NC: S-phase accumulation (**a**–**d**) as well as decreased G2/M proportions (**e**–**h**) were observed after combined treatment of different NC cell lines (143100, 690100, HCC2429, SNU-3178S) with NEO2734 and T-VEC. Monotherapy with NEO2734 induced a G1 arrest (**a**–**d**). Combination treatment also induced elevated Sub-G1 fractions (**i**–**l**). Cell cycle analysis was performed 48 hpt using propidium iodide (PI) staining and flow cytometry. All cell lines were treated with the IC_{50} of NEO2734 determined in preliminary experiments (Table S1) and infected with T-VEC at MOIs of (**a**,**e**,**i**) 0.00005, (**b**,**f**,**j**) 0.0005, (**c**,**g**,**k**) 0.001, and (**d**,**h**,**l**) 0.005, either in dual combination, individually, or remained untreated (MOCK). Data represent the mean ± SD from at least two independent experiments ($n \geq 2$). * $p < 0.05$, *ns* = not significant.

3.3. Analysis of Immunogenic Cell Death Markers

ICD is characterized by the coordinated release and extracellular exposure of ATP, HMGB1, and CALR, which act as key DAMPs mediating activation of the immune system [55]. In this study, these DAMPs were analyzed after combination treatment of T-VEC with NEO2734 in four distinct NC cell lines (143100, 690100, HCC2429, and SNU-3178S).

3.3.1. Extracellular ATP Analysis

To assess immunogenic cell death, the release of extracellular ATP was quantified as a marker of ICD. Cell culture supernatants were collected 72 hpt and analyzed using the CellTiter-Glo® luminescence assay (Figure 4). In the cell lines 143100, 690100, and HCC2429, combination treatment induced a significant increase in extracellular ATP levels

compared with the MOCK control ($p < 0.01$ to $p < 0.0001$). The most profound increase was observed in cell line 143100, where the ATP levels rose to 242.5% relative to MOCK. T-VEC monotherapy also resulted in a significant increase in extracellular ATP in cell line 690100, reaching 229% relative to MOCK ($p < 0.0001$), which was in the same range as the combination therapy. In contrast, no significant changes in ATP release were detected in the remaining cell lines following T-VEC treatment. In comparison, NEO2734 monotherapy led to a significant reduction in extracellular ATP across most analyzed cell lines (143100, HCC2429, and SNU-3178S) compared with MOCK ($p < 0.001$ to $p < 0.0001$). Cell line 690100 represented an exception, although a relevant downward trend was observed. In the cell line SNU-3178S, neither monotherapy nor combination treatment increased the extracellular ATP. Instead, T-VEC showed no measurable effect, whereas NEO2734 and combination treatment reduced ATP levels ($p < 0.001$).

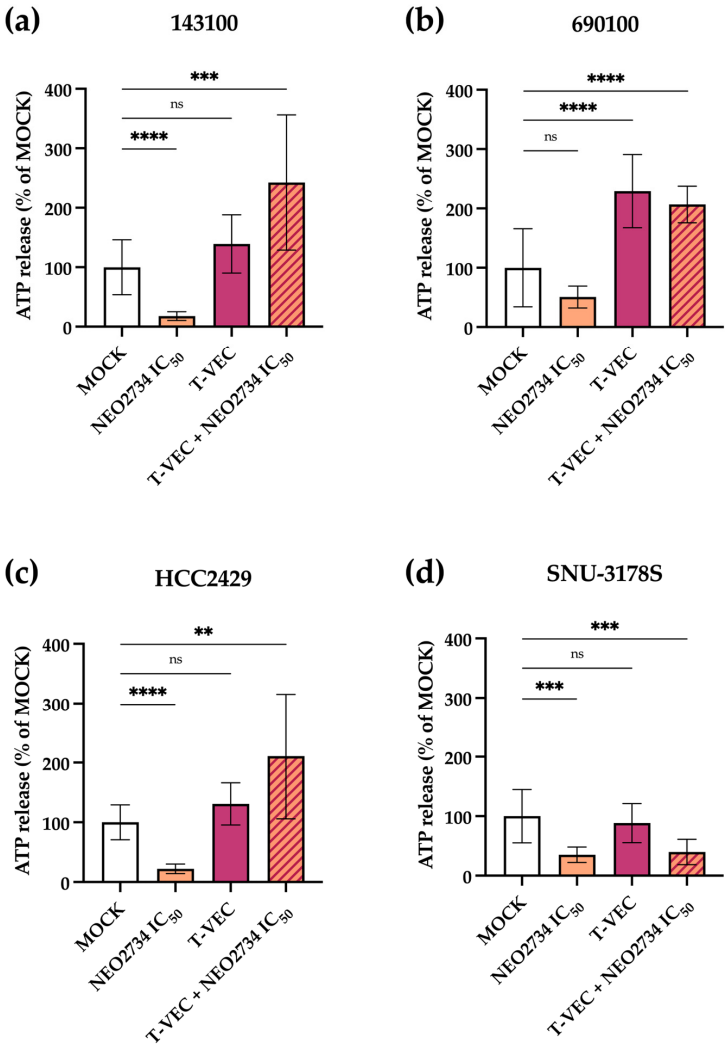


Figure 4. T-VEC alone and combination treatment with NEO2734 enhance ATP release in NC cells: Both T-VEC monotherapy and the combination of T-VEC with NEO2734 show increased ATP release in most NC cell lines (143100, 690100, HCC2429), whereas treatment with NEO2734 alone does not have this effect. Extracellular ATP was quantified 72 hpt with a CellTiter-Glo® assay. All cell lines (143100, 690100, HCC2429, and SNU-3178S) were treated with the IC_{50} of NEO2734 determined from preliminary experiments (Table S1) and infected with T-VEC at MOIs of (**a**) 0.00005, (**b**) 0.0005, (**c**) 0.001, and (**d**) 0.005, either in dual combination, individually, or remained untreated (MOCK). The mean ± SD of two independent experiments with four biological replicates ($n = 8$) is shown. Results are presented relative to MOCK control. ** $p < 0.01$, *** $p < 0.001$, **** $p < 0.0001$, *ns* = not significant.

3.3.2. Extracellular HMGB1 Analysis

Furthermore, HMGB1 release was quantitatively assessed 72 hpt using a Lumit® HMGB1 immunoassay as an additional marker of ICD (Figure 5). Across all analyzed cell lines, a trend toward increased HMGB1 release with virotherapy and combinatorial treatment compared with the MOCK control was observed. However, a statistically significant increase relative to MOCK was detected only in the cell line 690100 ($p = 0.0224$). NEO2734 monotherapy generally reduced extracellular HMGB1 levels compared to MOCK, although this reduction only reached statistical significance in cell line SNU-3178S ($p = 0.0029$). Comparison of NEO2734 treatment alone with T-VEC monotherapy revealed significant differences in extracellular HMGB1 in 143100, 690100, and SNU-3178S ($p < 0.01$ to $p < 0.0001$), with consistently higher HMGB1 levels observed following T-VEC treatment. No significant difference was detected in HCC2429 ($p = 0.2370$).

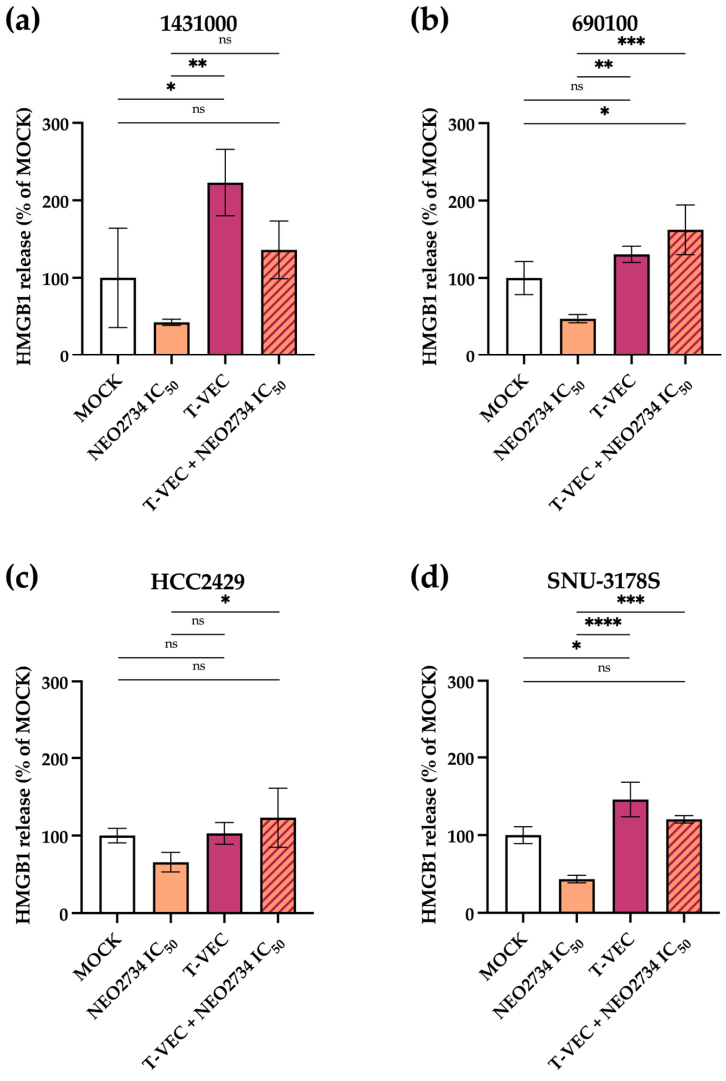


Figure 5. Extracellular HMGB1 release in NC cells after combinatorial treatment: Elevated extracellular HMGB1 (high mobility group box 1) levels were observed with combined treatment of NUT carcinoma cell lines (143100, 690100, HCC2429, SNU-3178S) with T-VEC and NEO2734 compared to NEO2734 monotherapy. HMGB1 levels were measured 72 hpt using the Lumit® HMGB1 Immunoassay. All cell lines were treated with the IC_{50} of NEO2734 determined from preliminary experiments (Table S1) and treated with T-VEC at an MOI of (**a**) 0.0001, (**b**) 0.0005, (**c**) 0.001, and (**d**) 0.005, either in dual combination, individually, or remained untreated (MOCK). The mean ± SD of three biological replicates, is shown ($n = 3$). Results are shown relative to MOCK control. * $p < 0.05$, ** $p < 0.01$, *** $p < 0.001$, **** $p < 0.0001$, *ns* = not significant.

Importantly, a significant increase in HMGB1 levels was seen with the addition of T-VEC to NEO2734 monotherapy in cell lines 690100, HCC2429, and SNU-3178S ($p < 0.05$ to $p < 0.001$). Nevertheless, no significant differences were detected between T-VEC monotherapy and the combination treatment.

3.3.3. Calreticulin Surface Expression

As a third marker of ICD, CALR expression on the cellular surface was assessed 48 hpt by flow cytometry (Figure 6). In three of the four analyzed cell lines (143100, 690100, and HCC2429), combination treatment induced a significant increase in CALR surface expression compared with the MOCK control ($p < 0.05$ to $p < 0.001$), whereas the respective monotherapies showed only minor effects. A similar trend was observed in SNU-3178S, with a relevant increase of 9.7% relative to MOCK, yet this difference did not reach statistical significance ($p = 0.0925$). The most pronounced increase in CALR surface expression following combination treatment was detected in cell line 143100, with an increase of 26.8%. Neither NEO2734 nor T-VEC monotherapy significantly altered CALR surface expression compared with MOCK, except for T-VEC treatment in HCC2429 ($p < 0.01$), where the observed effect remained lower than the one detected following combination treatment.

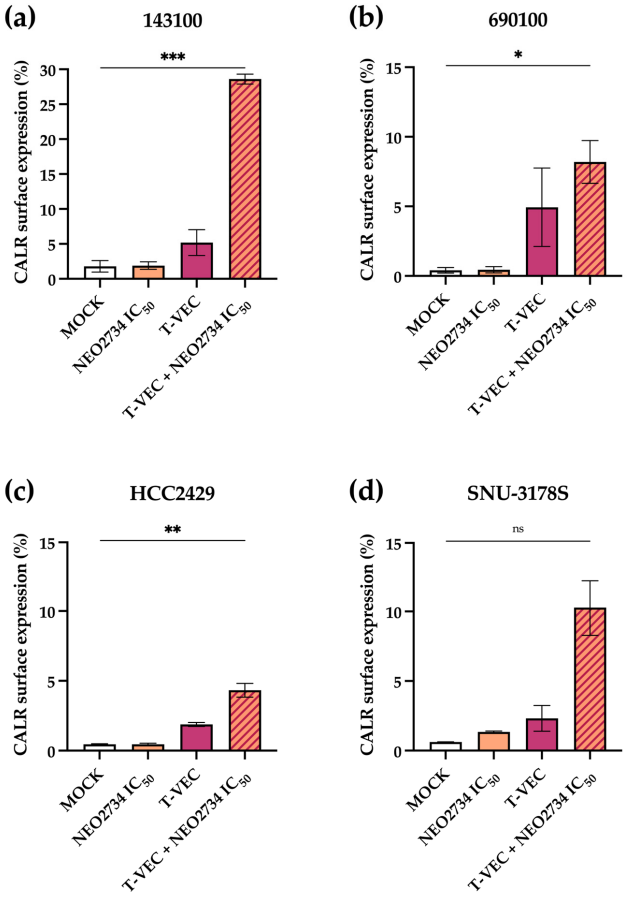


Figure 6. Calreticulin surface expression on NC cells after combined treatment of NC cells: Combined treatment of various NC cell lines (143100, 690100, HCC2429, SNU-3178S) with T-VEC and NEO2734 resulted in an increased expression of calreticulin (CALR) on the cell surface. CALR expression was measured 48 hpt by flow cytometry. All cell lines were treated with the IC_{50} concentrations of NEO2734 determined in preliminary experiments (Table S1) and infected with T-VEC at MOIs of (**a**) 0.00005, (**b**) 0.0005, (**c**) 0.001, and (**d**) 0.005, either in dual combination, individually, or left untreated (MOCK). The mean value ± SD of two independent experiments ($n = 2$), is shown. * $p < 0.05$, ** $p < 0.01$, *** $p < 0.001$, *ns* = not significant.

4. Discussion

To overcome the limitations of current therapeutic approaches, including emerging strategies such as small-molecule inhibitors (SMIs) and immunotherapies, in the treatment of the highly aggressive NUT carcinoma (NC), this study investigated a dual combination regimen consisting of an SMI combined with oncolytic viruses (OVs). Specifically, this approach aims to address the rapid development of resistance to SMIs and the difficulty of converting an immunologically "cold" tumor microenvironment into a "hot" immune-competent state [11,12,31,37,41].

Consistent with previous reports, the dual BET and p300/CBP inhibitor NEO2734 demonstrated high potency across multiple NC cell lines, with IC_{25} and IC_{50} values in the low nanomolar range (Figure S1 and Table S1), confirming its antitumoral activity [36]. As NEO2734 is currently under clinical evaluation (NCT05488548), it remains to be determined whether resistance mechanisms and treatment relevant toxicities similar to those described for other BET inhibitors will emerge and limit its long-term efficacy [31]. Based on existing data on BET inhibitors, which are commonly associated with thrombocytopenia and gastrointestinal adverse events [11], hematological toxicities such as cytopenia may also be anticipated for NEO2734, whereas the OV T-VEC has a well-established safety profile and is commonly associated with low-grade transient fever, chills and fatigue [49]. Resistance to BET inhibition has been linked to adaptive epigenetic reprogramming, including the activation of several compensatory signaling pathways, such as WNT β-catenin signaling, which sustain oncogenic programs like *MYC* expression [13,31]. While NEO2734 monotherapy has been shown to induce robust c-MYC downregulation [56,57], preclinical studies combining SMIs with OVs suggest that such combinations may promote a more rapid and sustained suppression of c-MYC, indicating mechanistic complementarity between epigenetic modulation and virus-mediated tumor targeting [44].

The rationale for combining SMIs with OVs is based on their temporally and mechanistically distinct antitumoral effects. While SMIs primarily exert antiproliferative effects through epigenetic modulation, OVs initially induce direct tumor cell lysis and subsequently promote a sustained in situ antitumor immune response. Their combination may provide complementary therapeutic effects and potentially delay the emergence of resistance [36,58,59]. In vitro studies further suggest that epigenetic modulators can enhance OV efficacy in NC by increasing cellular permissivity to viral infection. This effect may be mediated by chromatin remodeling and suppression of antiviral interferon responses, thereby facilitating viral entry, replication, and oncolysis [43,44]. However, the precise molecular mechanisms underlying this interaction remain to be fully elucidated.

The combination of NEO2734 with two distinct OVs, a measles vaccine virus (MeV-GFP) and the herpes simplex virus talimogene laherparepvec (T-VEC), resulted in predominantly additive to synergistic effects across NC cell lines. Among both tested combinations, T-VEC combined with NEO2734 demonstrated the more robust and consistent synergistic effects, particularly in the cell line 143100, but also in 690100 and SNU-3178S (Figures 1 and 2). Interestingly, synergistic interactions were more pronounced for T-VEC combinations at IC_{25} concentrations than at IC_{50} concentrations, suggesting biologically relevant interactions at specific dose ratios rather than nonspecific cytotoxicity (Figures 1 and 2). In contrast, combinations with MeV-GFP rather resulted in additive to slight synergistic effects (Figures 1 and 2). The reduced responsiveness of SNU-3178S to the MeV-GFP and NEO2734 combination suggests a lower susceptibility to this specific treatment (Figure 1d).

The heterogeneous responses observed across NC cell lines, particularly the exceptional sensitivity of 143100 cells to the T-VEC and NEO2734 combination, suggest an important role for tumor-specific factors. Such variability may be influenced by differences in interferon pathway competence, viral receptor expression, epigenetic regulation, or broader

genetic heterogeneity, including differences in *NUTM1* fusion partners (*BRD4*::*NUTM1* versus *BRD3*::*NUTM1*).

Despite these differences, all NC cell lines appeared permissive to viral infection, and combinatorial therapy was beneficial in all cases. These findings are consistent with other preclinical studies reporting enhanced and additive antitumoral effects of T-VEC-based combinations with BET or p300/CBP mono-inhibitors in NC, supporting the broader therapeutic potential of T-VEC in this disease; however, synergistic effects were not demonstrated in these studies [43,44]. The occasionally high standard deviations observed at very low multiplicities of infection (MOIs) likely reflect the technical variability associated with the use of low MOIs, which were chosen to preserve a sufficient dynamic range for detecting combinatorial effects.

The cell cycle analysis (Figure 3) suggests that NEO2734 primarily induces G1 cell cycle arrest, consistent with results of NEO2734 observed in multiple myeloma cell lines, which is linked to c-MYC downregulation and antiproliferative effects [56]. In contrast, treatment with T-VEC, alone or in combination with NEO2734, could be associated with an accumulation of cells in S phase, which may reflect increased replication stress, a phenomenon commonly observed during viral infection and often associated with DNA damage and impaired DNA repair, which promote viral replication and inhibit cellular proliferation [60–62]. Epigenetic modulation by NEO2734 could further exacerbate these effects, thereby contributing to the observed synergistic antitumoral activity. The reduction in the G2/M fraction and the increase in the sub-G1 population observed predominantly under combination treatment are consistent with enhanced cell death induction, possibly associated with oncolysis and apoptosis. However, confirmation of specific apoptotic mechanisms will require additional analyses, including caspase activation and annexin V staining [63].

Immunogenic cell death (ICD) represents a critical mechanism by which anticancer therapies can promote durable antitumor immunity, previously described for therapies with OVs. In this study, the detection of established ICD markers indicates that the combination therapy induces immunogenic signals beyond direct cytotoxicity, comparable to effects previously described for T-VEC in other tumor models [37,40–42,64].

Notably, increased extracellular ATP release following T-VEC and combination treatment (Figure 4) and HMGB1 secretion induced by T-VEC, which remains largely preserved in the combination therapy (Figure 5), were observed in most NC cell lines. While CALR surface exposure was significantly enhanced in three out of four cell lines, neither NEO2734 nor T-VEC alone induced comparable effects (Figure 6). In contrast, NEO2734 alone consistently reduced ICD marker levels, rather reflecting a primarily antiproliferative non-immunogenic mode of action, consistent with the G1 arrest, which inhibits cell proliferation without necessarily activating apoptotic or immunogenic cell death mechanisms [56]. SNU-3178S harboring a *BRD3*::*NUTM1* fusion showed the lowest overall positivity for ICD markers, suggesting that it is the least responsive to the induction of immunogenic cell death by the tested therapy. Collectively, fusion partner-dependent differences in tumor biology may contribute to reduced OV replication and attenuated ICD induction in this model. While previous studies have reported potential enhanced sensitivity to BET inhibition in non-*BRD4* NC cells [11], such increased sensitivity was not observed in this experimental setting. Nevertheless, the strong antiproliferative effects of dual BET/p300 inhibition, together with altered cell cycle regulation, reflected by a more pronounced G1-phase accumulation in SNU-3178S following combination treatment, may limit viral amplification and subsequent ICD induction. In contrast, the strong ICD marker profile and pronounced therapeutic synergy observed in cell line 143100 suggest a potential link between immunogenic cell response and high treatment efficacy. Overall, the combination

treatment yielded heterogenous cell-line dependent effects, precluding the assumption of a consistent synergistic increase in ATP or HMGB1 release. In contrast, CALR surface exposure appeared to be synergistically enhanced by the combination. While ICD marker induction provides functional mechanistic insight and may be influenced by cell-intrinsic factors, including epigenetic state and *NUTM1* variants, the exact molecular pathways linking epigenetic modulation and OV-induced ICD remain to be fully elucidated. As CALR exposure has been associated with improved clinical outcomes in other malignancies, where it serves as a prognostic marker [65], ecto-CALR may represent a potential prognostic biomarker for NEO2734/T-VEC combination therapies. Given the limited sample size for some analyses, caution is warranted in interpreting these data and drawing statistically conclusive comparisons between cell lines. However, the observed patterns were consistent across multiple ICD makers and aligned with the robust cytotoxic and synergistic effects observed in independent assays, supporting the biological relevance of the findings. As the study is conducted in vitro, the influence of the immune system on the antitumor efficacy and immunity to different OVs remains unclear. Therefore, translation into antitumor effects in a living host have to be made with caution. Taken together, this combinatorial therapy significantly enhances DAMP release which lies the foundation for a therapeutic OV-induced antitumoral immune response in vivo.

5. Conclusions

In summary, the combination of NEO2734 with OVs, particularly T-VEC, represents a promising multimodal therapeutic option for the treatment of the highly aggressive NC, for which effective treatment strategies are currently lacking [4,18]. The use of lower doses of both modalities in synergistic combinations could reduce dose-limiting toxicities while maximizing the therapeutic efficacy [66]. Synergistic cytotoxic effects as well as a profound induction of ICD could be demonstrated for the combination of NEO2734 and T-VEC. Future studies should prioritize in vivo validation to assess the contribution of the immune system to therapeutic response, identify predictive biomarkers of treatment sensitivity, and evaluate the durability of antitumor immunity. Genetically engineered mouse models harboring *BRD4*::*NUTM1* fusions [67], as well as patient-derived organoid models [48], represent suitable platforms to further advance the translational potential of this combination strategy. Together, these findings provide a strong rationale for further development of the combination of NEO2734 and T-VEC in NC, including validation in additional NC models with distinct *NUTM1* fusion variants and the evaluation of alternative OVs.

Supplementary Materials: The following supporting information can be downloaded at https://www.mdpi.com/article/10.3390/v18020267/s1, Figure S1: Monotherapy of NUT carcinoma (NC) cells with NEO2734; Figure S2: Representative phase contrast and fluorescence microscopy images of treated NC cell lines; Figure S3: Heatmaps of ZIP synergy scores for combination treatments in NC cell lines; Figure S4: Representative gating strategy for cell cycle analysis by flow cytometry in the untreated cell line 143100; Figure S5: Representative gating strategy to quantify CALR surface expression by flow cytometry; Table S1: Calculated IC_{25} and IC_{50} values of NC cells treated with NEO2734; Table S2: Multiplicities of infection (MOIs) used for each NC cell line and oncolytic virus; Table S3: Synergy Scores (ZIP, Loewe, HSA, and Bliss) for all tested combinations across the indicated cell lines.

Author Contributions: Conceptualization, U.M.L. and L.D.K.; validation, J.B., M.E.C., U.M.L. and L.D.K.; methodology, F.D.N., U.M.L. and L.D.K.; formal analysis, F.D.N. and L.D.K.; investigation, F.D.N., I.S. and A.S.; resources, U.M.L.; writing—original draft preparation, F.D.N.; writing—review and editing, J.B., M.E.C., U.M.L. and L.D.K.; visualization, F.D.N.; supervision, U.M.L. and L.D.K.;

project administration, L.D.K.; funding acquisition, U.M.L. and L.D.K. All authors have read and agreed to the published version of the manuscript.

Funding: This research was funded by the Deutsche Forschungsgemeinschaft (DFG, German Research Foundation)—514598620. L.D.K. and M.E.C. were funded by the intramural fortüne program of the Faculty of Medicine, University of Tuebingen (proposal numbers 3007-0-0 and 3033-0-0).

Institutional Review Board Statement: Not applicable as this work was conducted with previously published or commercially available cell lines.

Informed Consent Statement: Not applicable.

Data Availability Statement: The original contributions presented in this study are included in the article/Supplementary Materials. Further inquiries can be directed to the corresponding author(s).

Acknowledgments: We also acknowledge support from the Open Access Publishing Fund of the University of Tübingen. The graphical abstract was created using BioRender.com [68].

Conflicts of Interest: The authors declare no conflicts of interest.

Abbreviations

The following abbreviations are used in this manuscript:

ANOVA	Analysis of variance
ATP	Adenosine triphosphate
BET	Bromodomain and extra-terminal domain
BRD3/4	Bromodomain containing protein 3 or 4
CALR	Calreticulin
Cas9	CRISPR-associated protein 9
CBP	CREB-binding protein
CDK	Cyclin-dependent kinase
CREB	cAMP response element-binding protein
CRISPR	Clustered regularly interspaced short palindromic repeats
DAMP	Damage-associated molecular pattern
DFG	Deutsche Forschungsgemeinschaft
DMEM	Dulbecco's modified eagle's medium
EDTA	Ethylenediaminetetraacetic acid
FACS	Fluorescence-activated cell sorting
FBS	Fetal bovine serum
FDA	Food and Drug Administration
GFP	Green fluorescent protein
GM-CSF	Granulocyte macrophage colony-stimulating factor
HDACi	Histone deacetylase inhibitor
HMGB1	High mobility group box 1
Hpi	Hours post infection
Hpt	Hours post treatment
HSA	Highest single agent
HSV-1	Herpes simplex virus type 1
$IC_{25/50}$	Inhibitory concentration 25 or 50
ICD	Immunogenic cell death
ICI	Immune checkpoint inhibitors
ICP	Infected cell protein
MeV	Measles vaccine virus
MOI	Multiplicities of infection
MYC	Proto-oncogene
NC	NUT carcinoma
NS	Not significant

NSD3	Nuclear receptor binding SET domain protein 3
NUT	Nuclear-protein-in-testis
NUTM1	NUT midline carcinoma family member 1
OS	Overall survival
OV	Oncolytic virus
PBS	Phosphate buffered saline
PD-L1	Programmed death-ligand 1
PFA	Paraformaldehyde
PI	Propidium iodide
RT	Room temperature
SD	Standard deviation
SOX2	SRY (sex determining region Y)-box 2
SMI	Small-molecule inhibitor
SRB	Sulforhodamine B
TCA	Trichloroacetic acid
TMB	Tumor mutation burden
TME	Tumor microenvironment
T-VEC	Talimogene laherparepvec
TP63	Tumor protein p63
ZIP	Zero interaction potency

References

1. French, C.A. NUT Carcinoma: Clinicopathologic features, pathogenesis, and treatment. *Pathol. Int.* **2018**, *68*, 583–595. [CrossRef]
2. Bishop, J.A.; French, C.A.; Ali, S.Z. Cytopathologic features of NUT midline carcinoma: A series of 26 specimens from 13 patients. *Cancer Cytopathol.* **2016**, *124*, 901–908. [CrossRef] [PubMed]
3. French, C.A.; Miyoshi, I.; Kubonishi, I.; Grier, H.E.; Perez-Atayde, A.R.; Fletcher, J.A. BRD4-NUT fusion oncogene: A novel mechanism in aggressive carcinoma. *Cancer Res.* **2003**, *63*, 304–307. [PubMed]
4. Chau, N.G.; Ma, C.; Danga, K.; Al-Sayegh, H.; Nardi, V.; Barrette, R.; Lathan, C.S.; DuBois, S.G.; Haddad, R.I.; Shapiro, G.I.; et al. An Anatomical Site and Genetic-Based Prognostic Model for Patients With Nuclear Protein in Testis (NUT) Midline Carcinoma: Analysis of 124 Patients. *JNCI Cancer Spectr.* **2020**, *4*, pkz094. [CrossRef] [PubMed]
5. Moreno, V.; Saluja, K.; Pina-Oviedo, S. NUT Carcinoma: Clinicopathologic Features, Molecular Genetics and Epigenetics. *Front. Oncol.* **2022**, *12*, 860830. [CrossRef]
6. French, C.A.; Ramirez, C.L.; Kolmakova, J.; Hickman, T.T.; Cameron, M.J.; Thyne, M.E.; Kutok, J.L.; Toretsky, J.A.; Tadavarthy, A.K.; Kees, U.R.; et al. BRD-NUT oncoproteins: A family of closely related nuclear proteins that block epithelial differentiation and maintain the growth of carcinoma cells. *Oncogene* **2008**, *27*, 2237–2242. [CrossRef]
7. French, C.A.; Rahman, S.; Walsh, E.M.; Kühnle, S.; Grayson, A.R.; Lemieux, M.E.; Grunfeld, N.; Rubin, B.P.; Antonescu, C.R.; Zhang, S.; et al. NSD3-NUT fusion oncoprotein in NUT midline carcinoma: Implications for a novel oncogenic mechanism. *Cancer Discov.* **2014**, *4*, 928–941. [CrossRef]
8. Narita, T.; Ito, S.; Higashijima, Y.; Chu, W.K.; Neumann, K.; Walter, J.; Satpathy, S.; Liebner, T.; Hamilton, W.B.; Maskey, E.; et al. Enhancers are activated by p300/CBP activity-dependent PIC assembly, RNAPII recruitment, and pause release. *Mol. Cell* **2021**, *81*, 2166–2182.e2166. [CrossRef]
9. Reynoird, N.; Schwartz, B.E.; Delvecchio, M.; Sadoul, K.; Meyers, D.; Mukherjee, C.; Caron, C.; Kimura, H.; Rousseaux, S.; Cole, P.A.; et al. Oncogenesis by sequestration of CBP/p300 in transcriptionally inactive hyperacetylated chromatin domains. *EMBO J.* **2010**, *29*, 2943–2952. [CrossRef]
10. French, C.A. Pathogenesis of NUT midline carcinoma. *Annu. Rev. Pathol.* **2012**, *7*, 247–265. [CrossRef]
11. French, C.A.; Cheng, M.L.; Hanna, G.J.; DuBois, S.G.; Chau, N.G.; Hann, C.L.; Storck, S.; Salgia, R.; Trucco, M.; Tseng, J.; et al. Report of the First International Symposium on NUT Carcinoma. *Clin. Cancer Res.* **2022**, *28*, 2493–2505. [CrossRef] [PubMed]
12. Eagen, K.P.; French, C.A. Supercharging BRD4 with NUT in carcinoma. *Oncogene* **2021**, *40*, 1396–1408. [CrossRef] [PubMed]
13. Alekseyenko, A.A.; Walsh, E.M.; Wang, X.; Grayson, A.R.; Hsi, P.T.; Kharchenko, P.V.; Kuroda, M.I.; French, C.A. The oncogenic BRD4-NUT chromatin regulator drives aberrant transcription within large topological domains. *Genes Dev.* **2015**, *29*, 1507–1523. [CrossRef] [PubMed]
14. Lemelle, L.; Moya-Plana, A.; Dumont, B.; Fresneau, B.; Laprie, A.; Claude, L.; Deneuve, S.; Cordero, C.; Pierron, G.; Couloigner, V.; et al. NUT carcinoma in children, adolescents and young adults. *Bull. Cancer* **2022**, *109*, 491–504. [CrossRef]

15. Chau, N.G.; Hurwitz, S.; Mitchell, C.M.; Aserlind, A.; Grunfeld, N.; Kaplan, L.; Hsi, P.; Bauer, D.E.; Lathan, C.S.; Rodriguez-Galindo, C.; et al. Intensive treatment and survival outcomes in NUT midline carcinoma of the head and neck. *Cancer* **2016**, *122*, 3632–3640. [CrossRef]
16. You, Y.; Lu, S.; Sun, F.; He, X.; Wang, J.; Huang, J.; Que, Y.; Zhen, Z.; Zhang, Y.; Zhu, J. Pediatric NUT carcinoma: A patient series and literature review. *BMC Pediatr.* **2025**, *25*, 889. [CrossRef]
17. Beesley, A.H.; Stirnweiss, A.; Ferrari, E.; Endersby, R.; Howlett, M.; Failes, T.W.; Arndt, G.M.; Charles, A.K.; Cole, C.H.; Kees, U.R. Comparative drug screening in NUT midline carcinoma. *Br. J. Cancer* **2014**, *110*, 1189–1198. [CrossRef]
18. Bauer, D.E.; Mitchell, C.M.; Strait, K.M.; Lathan, C.S.; Stelow, E.B.; Lüer, S.C.; Muhammed, S.; Evans, A.G.; Sholl, L.M.; Rosai, J.; et al. Clinicopathologic features and long-term outcomes of NUT midline carcinoma. *Clin. Cancer Res.* **2012**, *18*, 5773–5779. [CrossRef]
19. Yang, G.; Liu, R.; Yang, L.; Yang, X.; Tang, X.; Mao, H. Pulmonary NUT carcinoma, an elusive and refractory entity, shows transient response to chemotherapeutics and PD-1 inhibitor: A case report and literature review. *Front. Immunol.* **2025**, *16*, 1497124. [CrossRef]
20. Kloker, L.D.; Sidiras, M.; Flaadt, T.; Brecht, I.B.; Deinzer, C.K.W.; Groß, T.; Benzler, K.; Zender, L.; Lauer, U.M. Clinical management of NUT carcinoma (NC) in Germany: Analysis of survival, therapy response, tumor markers and tumor genome sequencing in 35 adult patients. *Lung Cancer* **2024**, *189*, 107496. [CrossRef]
21. Haebe, S.; Schuebbe, G.; Jurmeister, P.; von Bergwelt-Baildon, M.; Westphalen, C.B.; Lauer, U.M.; Kunz, W.G.; Subklewe, M.; Weigert, O. Adding checkpoint inhibitors to first-line chemotherapy for NUT carcinoma patients. *NPJ Precis. Oncol.* **2025**, *9*, 26. [CrossRef]
22. Riess, J.W.; Rahman, S.; Kian, W.; Edgerly, C.; Heilmann, A.M.; Madison, R.; Ramkissoon, S.H.; Klaitman, S.S.; Chung, J.H.; Trabucco, S.E.; et al. Genomic profiling of solid tumors harboring BRD4-NUT and response to immune checkpoint inhibitors. *Transl. Oncol.* **2021**, *14*, 101184. [CrossRef] [PubMed]
23. Chen, M.; Chen, X.; Zhang, Y.; Wang, W.; Jiang, L. Clinical and molecular features of pulmonary NUT carcinoma characterizes diverse responses to immunotherapy, with a pathologic complete response case. *J. Cancer Res. Clin. Oncol.* **2023**, *149*, 6361–6370. [CrossRef] [PubMed]
24. Qu, J.; Chen, Z.; Zhu, Y.; Huang, J.; Shen, Q. Pulmonary Nuclear protein in Testis (NUT) carcinoma: Clinical, molecular characteristics, and treatment strategies. *BMC Cancer* **2025**, *25*, 196. [CrossRef] [PubMed]
25. Kim, J.J.; Walton, S.A.; Mahadevan, N.R.; Haradon, J.; Paoloni, F.; Paik, P.K.; Chaft, J.E.; Hsu, R.; Piha-Paul, S.A.; Jänne, P.A.; et al. Molecular Characterization of NUT Carcinoma: A Report from the NUT Carcinoma Registry. *Clin. Cancer Res.* **2025**, *31*, 3922–3931. [CrossRef]
26. Carle, M.F.; Mohammadian Gol, T.; Antony, J.S.; Roig-Merino, A.; Carter, M.E.; Lauer, U.M.; Mezger, M.; Kloker, L.D. Targeting oncogenic fusion-driven NUT carcinoma with CRISPR-Cas9 genome editing. *Mol. Ther. Oncol.* **2025**, *33*, 201068. [CrossRef]
27. Lee, M.S.; An, S.; Song, J.Y.; Sung, M.; Jung, K.; Chang, E.S.; Choi, J.; Oh, D.Y.; Jeon, Y.K.; Yang, H.; et al. Cancer-Specific Sequences in the Diagnosis and Treatment of NUT Carcinoma. *Cancer Res. Treat.* **2023**, *55*, 452–467. [CrossRef]
28. Gen, Y.; Muramatsu, T.; Inoue, J.; Inazawa, J. miR-766-5p Targets Super-Enhancers by Downregulating CBP and BRD4. *Cancer Res.* **2021**, *81*, 5190–5201. [CrossRef]
29. Lauer, U.M.; Hinterleitner, M.; Horger, M.; Ohnesorge, P.V.; Zender, L. NUT Carcinoma-An Underdiagnosed Malignancy. *Front. Oncol.* **2022**, *12*, 914031. [CrossRef]
30. Kaplan, H.G.; Subramaniam, S.; Vallières, E.; Barnett, T. Prolonged Survival of NUT Midline Carcinoma and Current Approaches to Treatment. *Oncologist* **2023**, *28*, 765–770. [CrossRef]
31. Wang, S.; Li, J.; Tong, W.; Li, H.; Feng, Q.; Teng, B. Advances in the pathogenesis and treatment of nut carcinoma: A narrative review. *Transl. Cancer Res.* **2020**, *9*, 6505–6515. [CrossRef]
32. Cousin, S.; Blay, J.Y.; Garcia, I.B.; de Bono, J.S.; Le Tourneau, C.; Moreno, V.; Trigo, J.; Hann, C.L.; Azad, A.A.; Im, S.A.; et al. Safety, pharmacokinetic, pharmacodynamic and clinical activity of molibresib for the treatment of nuclear protein in testis carcinoma and other cancers: Results of a Phase I/II open-label, dose escalation study. *Int. J. Cancer* **2022**, *150*, 993–1006. [CrossRef] [PubMed]
33. Shapiro, G.I.; LoRusso, P.; Dowlati, A.; Do, K.T.; Jacobson, C.A.; Vaishampayan, U.; Weise, A.; Caimi, P.F.; Eder, J.P.; French, C.A.; et al. A Phase 1 study of RO6870810, a novel bromodomain and extra-terminal protein inhibitor, in patients with NUT carcinoma, other solid tumours, or diffuse large B-cell lymphoma. *Br. J. Cancer* **2021**, *124*, 744–753. [CrossRef] [PubMed]
34. Pearson, A.D.; DuBois, S.G.; Buenger, V.; Kieran, M.; Stegmaier, K.; Bandopadhayay, P.; Bennett, K.; Bourdeaut, F.; Brown, P.A.; Chesler, L.; et al. Bromodomain and extra-terminal inhibitors-A consensus prioritisation after the Paediatric Strategy Forum for medicinal product development of epigenetic modifiers in children-ACCELERATE. *Eur. J. Cancer* **2021**, *146*, 115–124. [CrossRef]
35. Huang, Y.; Durall, R.T.; Luong, N.M.; Hertzler, H.J.; Huang, J.; Gokhale, P.C.; Leeper, B.A.; Persky, N.S.; Root, D.E.; Anekal, P.V.; et al. EZH2 Cooperates with BRD4-NUT to Drive NUT Carcinoma Growth by Silencing Key Tumor Suppressor Genes. *Cancer Res.* **2023**, *83*, 3956–3973. [CrossRef]

36. Morrison-Smith, C.D.; Knox, T.M.; Filic, I.; Soroko, K.M.; Eschle, B.K.; Wilkens, M.K.; Gokhale, P.C.; Giles, F.; Griffin, A.; Brown, B.; et al. Combined Targeting of the BRD4-NUT-p300 Axis in NUT Midline Carcinoma by Dual Selective Bromodomain Inhibitor, NEO2734. *Mol. Cancer Ther.* **2020**, *19*, 1406–1414. [CrossRef]
37. Lauer, U.M.; Beil, J. Oncolytic viruses: Challenges and considerations in an evolving clinical landscape. *Future Oncol.* **2022**. [CrossRef] [PubMed]
38. Pikor, L.A.; Bell, J.C.; Diallo, J.S. Oncolytic Viruses: Exploiting Cancer's Deal with the Devil. *Trends Cancer* **2015**, *1*, 266–277. [CrossRef]
39. Russell, S.J.; Peng, K.W.; Bell, J.C. Oncolytic virotherapy. *Nat. Biotechnol.* **2012**, *30*, 658–670. [CrossRef]
40. Palanivelu, L.; Liu, C.H.; Lin, L.T. Immunogenic cell death: The cornerstone of oncolytic viro-immunotherapy. *Front. Immunol.* **2022**, *13*, 1038226. [CrossRef]
41. Kaufman, H.L.; Kohlhapp, F.J.; Zloza, A. Oncolytic viruses: A new class of immunotherapy drugs. *Nat. Rev. Drug Discov.* **2015**, *14*, 642–662. [CrossRef] [PubMed]
42. Alwithenani, A.; Hengswat, P.; Chiocca, E.A. Oncolytic viruses as cancer therapeutics: From mechanistic insights to clinical translation. *Mol. Ther.* **2025**, *33*, 2217–2228. [CrossRef] [PubMed]
43. Ohnesorge, P.V.; Berchtold, S.; Beil, J.; Haas, S.A.; Smirnow, I.; Schenk, A.; French, C.A.; Luong, N.M.; Huang, Y.; Fehrenbacher, B.; et al. Efficacy of Oncolytic Herpes Simplex Virus T-VEC Combined with BET Inhibitors as an Innovative Therapy Approach for NUT Carcinoma. *Cancers* **2022**, *14*, 2761. [CrossRef]
44. Sotiriadis, S.; Beil, J.; Berchtold, S.; Smirnow, I.; Schenk, A.; Lauer, U.M. Multimodal Therapy Approaches for NUT Carcinoma by Dual Combination of Oncolytic Virus Talimogene Laherparepvec with Small Molecule Inhibitors. *Viruses* **2024**, *16*, 775. [CrossRef] [PubMed]
45. Kloker, L.D.; Calukovic, B.; Benzler, K.; Golf, A.; Böhm, S.; Günther, S.; Horger, M.; Haas, S.; Berchtold, S.; Beil, J.; et al. Case report: Immunovirotherapy as a novel add-on treatment in a patient with thoracic NUT carcinoma. *Front. Oncol.* **2022**, *12*, 995744. [CrossRef]
46. Berchtold, S.; Lampe, J.; Weiland, T.; Smirnow, I.; Schleicher, S.; Handgretinger, R.; Kopp, H.G.; Reiser, J.; Stubenrauch, F.; Mayer, N.; et al. Innate immune defense defines susceptibility of sarcoma cells to measles vaccine virus-based oncolysis. *J. Virol.* **2013**, *87*, 3484–3501. [CrossRef]
47. Scheubeck, G.; Berchtold, S.; Smirnow, I.; Schenk, A.; Beil, J.; Lauer, U.M. Starvation-Induced Differential Virotherapy Using an Oncolytic Measles Vaccine Virus. *Viruses* **2019**, *11*, 614. [CrossRef]
48. Carter, M.E.; Hartkopf, A.D.; Wagner, A.; Volmer, L.L.; Brucker, S.Y.; Berchtold, S.; Lauer, U.M.; Koch, A. A Three-Dimensional Organoid Model of Primary Breast Cancer to Investigate the Effects of Oncolytic Virotherapy. *Front. Mol. Biosci.* **2022**, *9*, 826302. [CrossRef]
49. Andtbacka, R.H.; Kaufman, H.L.; Collichio, F.; Amatruda, T.; Senzer, N.; Chesney, J.; Delman, K.A.; Spitler, L.E.; Puzanov, I.; Agarwala, S.S.; et al. Talimogene Laherparepvec Improves Durable Response Rate in Patients With Advanced Melanoma. *J. Clin. Oncol.* **2015**, *33*, 2780–2788. [CrossRef]
50. Conry, R.M.; Westbrook, B.; McKee, S.; Norwood, T.G. Talimogene laherparepvec: First in class oncolytic virotherapy. *Hum. Vaccines Immunother.* **2018**, *14*, 839–846. [CrossRef]
51. Promega. CellTiter-Glo® Luminescent Cell Viability Assay. Available online: https://www.promega.de/products/cell-health-assays/cell-viability-and-cytotoxicity-assays/celltiter_glo-luminescent-cell-viability-assay/?catNum=G7571 (accessed on 6 November 2025).
52. Promega. Lumit® HMGB1 (Human/Mouse) Immunoassay. Available online: https://www.promega.de/en/products/cell-health-assays/inflammation-assay/lumit-hmgb1-human-mouse-immunoassay/?catNum=W6110 (accessed on 6 November 2025).
53. Liu, P.; Zhao, L.; Kepp, O.; Kroemer, G. Quantitation of calreticulin exposure associated with immunogenic cell death. *Methods Enzymol.* **2020**, *632*, 1–13. [CrossRef] [PubMed]
54. Zheng, S.; Wang, W.; Aldahdooh, J.; Malyutina, A.; Shadbahr, T.; Tanoli, Z.; Pessia, A.; Tang, J. SynergyFinder Plus: Toward Better Interpretation and Annotation of Drug Combination Screening Datasets. *Genom. Proteom. Bioinform.* **2022**, *20*, 587–596. [CrossRef] [PubMed]
55. Fucikova, J.; Kepp, O.; Kasikova, L.; Petroni, G.; Yamazaki, T.; Liu, P.; Zhao, L.; Spisek, R.; Kroemer, G.; Galluzzi, L. Detection of immunogenic cell death and its relevance for cancer therapy. *Cell Death Dis.* **2020**, *11*, 1013. [CrossRef] [PubMed]
56. Ryan, K.R.; Giles, F.; Morgan, G.J. Targeting both BET and CBP/EP300 proteins with the novel dual inhibitors NEO2734 and NEO1132 leads to anti-tumor activity in multiple myeloma. *Eur. J. Haematol.* **2021**, *106*, 90–99. [CrossRef]
57. Spriano, F.; Gaudio, E.; Cascione, L.; Tarantelli, C.; Melle, F.; Motta, G.; Priebe, V.; Rinaldi, A.; Golino, G.; Mensah, A.A.; et al. Antitumor activity of the dual BET and CBP/EP300 inhibitor NEO2734. *Blood Adv.* **2020**, *4*, 4124–4135. [CrossRef]
58. Spiesschaert, B.; Angerer, K.; Park, J.; Wollmann, G. Combining Oncolytic Viruses and Small Molecule Therapeutics: Mutual Benefits. *Cancers* **2021**, *13*, 3386. [CrossRef]

59. Chianese, A.; Santella, B.; Ambrosino, A.; Stelitano, D.; Rinaldi, L.; Galdiero, M.; Zannella, C.; Franci, G. Oncolytic Viruses in Combination Therapeutic Approaches with Epigenetic Modulators: Past, Present, and Future Perspectives. *Cancers* **2021**, *13*, 2761. [CrossRef]
60. Bagga, S.; Bouchard, M.J. Cell cycle regulation during viral infection. *Methods Mol. Biol.* **2014**, *1170*, 165–227. [CrossRef]
61. Nickoloff, J.A.; Jaiswal, A.S.; Sharma, N.; Williamson, E.A.; Tran, M.T.; Arris, D.; Yang, M.; Hromas, R. Cellular Responses to Widespread DNA Replication Stress. *Int. J. Mol. Sci.* **2023**, *24*, 16903. [CrossRef]
62. Panda, M.; Kalita, E.; Rao, A.; Prajapati, V.K. Mechanism of cell cycle regulation and cell proliferation during human viral infection. *Adv. Protein Chem. Struct. Biol.* **2023**, *135*, 497–525. [CrossRef]
63. Babes, R.M.; Tofolean, I.T.; Sandu, R.G.; Baran, O.E.; Cosoreanu, V.; Ilie, M.T.; Duta, A.I.; Ceausescu, M.C.; Ciucur, P.M.; Costache, S.; et al. Simple discrimination of sub-cycling cells by propidium iodide flow cytometric assay in Jurkat cell samples with extensive DNA fragmentation. *Cell Cycle* **2018**, *17*, 766–779. [CrossRef]
64. Kohlhapp, F.J.; Kaufman, H.L. Molecular Pathways: Mechanism of Action for Talimogene Laherparepvec, a New Oncolytic Virus Immunotherapy. *Clin. Cancer Res.* **2016**, *22*, 1048–1054. [CrossRef]
65. Fucikova, J.; Truxova, I.; Hensler, M.; Becht, E.; Kasikova, L.; Moserova, I.; Vosahlikova, S.; Klouckova, J.; Church, S.E.; Cremer, I.; et al. Calreticulin exposure by malignant blasts correlates with robust anticancer immunity and improved clinical outcome in AML patients. *Blood* **2016**, *128*, 3113–3124. [CrossRef]
66. Sun, Y.; Han, J.; Wang, Z.; Li, X.; Sun, Y.; Hu, Z. Safety and Efficacy of Bromodomain and Extra-Terminal Inhibitors for the Treatment of Hematological Malignancies and Solid Tumors: A Systematic Study of Clinical Trials. *Front. Pharmacol.* **2020**, *11*, 621093. [CrossRef]
67. Durall, R.T.; Huang, J.; Wojenski, L.; Huang, Y.; Gokhale, P.C.; Leeper, B.A.; Nash, J.O.; Ballester, P.L.; Davidson, S.; Shlien, A.; et al. The BRD4-NUT Fusion Alone Drives Malignant Transformation of NUT Carcinoma. *Cancer Res.* **2023**, *83*, 3846–3860. [CrossRef]
68. BioRender.com. Available online: https://www.biorender.com (accessed on 12 January 2026).

Disclaimer/Publisher's Note: The statements, opinions and data contained in all publications are solely those of the individual author(s) and contributor(s) and not of MDPI and/or the editor(s). MDPI and/or the editor(s) disclaim responsibility for any injury to people or property resulting from any ideas, methods, instructions or products referred to in the content.